 ©2026 Uspekhi Fizicheskikh Nauk, Russian Academy of Sciences

CONFERENCES AND SYMPOSIA

PACS numbers: 87.19.xj, **87.55. – x, 87.56. – v**

Radiation medical physics *

A.P. Chernyaev, E.N. Lykova, F.R. Studenikin,
A.A. Shcherbakov, A.A. Kim, M.V. Zheltonozhskaya

DOI: https://doi.org/10.3367/UFNe.2025.05.040012

Contents

1. Introduction **664**

2. Methods for improving the efficacy of radiotherapy and diagnostic imaging **668**

2.1 Uncertainties in the physical factors of diagnostic imaging and radiotherapy; 2.2 Uncertainties in diffusion-weighted magnetic resonance imaging; 2.3 Transit dosimetry using detectors built into the TomoTherapy system; 2.4 A method for irradiating large tumors with TomoTherapy and Elekta Synergy accelerators; 2.5 Physical and technical studies for synchrotron-based proton radiotherapy; 2.6 Production of radionuclides for nuclear medicine using electron accelerators; 2.7 Development of domestic radiotherapy systems

3. Radiation sterilization of bone implants, medical devices, and food products **675**

4. A continuous education system for medical physicists **676**

5. Conclusion **677**

References **679**

Abstract. This review presents the origin, development, and objectives of the new field of "Radiation Medical Physics." The fundamental physical ideas underlying high-tech medical methods for the treatment of oncological malignancies and some of the most relevant areas of fundamental research in the field of radiation technologies for medicine are discussed. The results of joint work conducted by Moscow University and leading oncology centers in Moscow and Russia, which have gained wide recognition and are used to treat patients, are shown. The only Russian multi-stage system for training medical physicists working in radiotherapy departments of oncology centers and the role of Moscow University in the development of this educational and scientific field are described.

Keywords: radiation, dose, radiotherapy, nuclear medicine, radionuclide diagnostics, therapeutic interval

1. Introduction

The history of medical physics is closely linked to the translation of discoveries in fundamental physics into methods for diagnosing and treating disease. The discovery of X-rays by W.C. Röntgen in 1895 [1] and radioactivity by H. Becquerel in 1896 [2] made it possible to visualize internal organs without surgery. In 1896, the American physicist E.H. Grubbe performed the world's first radiotherapy procedure on a patient with an inoperable breast tumor [3] (Fig. 1a). At almost the same time, radiation began to be used in Europe to treat malignant tumors following the discovery of the radioactive elements polonium and radium by Pierre and Marie Curie [4]. By the beginning of the twentieth century, the first attempts had been made to use radioactive isotopes for brachytherapy [5]. In 1901, the French physician H.A. Danlos used radioisotopes to treat a tumor [6]. Figure 1b shows the placement of radium sources for the treatment of skin cancer.

These discoveries laid the foundations for the physics of ionizing-radiation interactions with matter, on which today's diagnostic and therapeutic methods were subsequently built. Their development relied on calculations and physical models of the transport, scattering, and absorption of different types of particles in biological media.

The first clinical uses of X-rays and radioactive substances were accompanied by a high incidence of complications because the biological effects of ionizing radiation were poorly understood and the delivered doses were not quantified [7, 8]. Cases of radiation burns, other complications, and even deaths following patient overexposure had already been documented by the beginning of the twentieth century [8]. Radiation burns and dermatitis also occurred among physicians and operators of radiotherapy equipment who did not understand the physics of ionizing-radiation interactions with biological tissue. For example, the review in [9] describes more than 80 cases of burns among radiologists. These events created an urgent need for quantitative methods of absorbed-dose control and for physicists capable of ensuring the accuracy and safety of medical procedures.

A.P. Chernyaev (*), **E.N. Lykova, F.R. Studenikin, A.A. Shcherbakov, A.A. Kim, M.V. Zheltonozhskaya**
Lomonosov Moscow state University,
Leninskie gory 1, str. 2, 119991 Moscow, Russian Federation
E-mail: (*)a.p.chernyaev@yandex.ru

Received 8 August 2025
Uspekhi Fizicheskikh Nauk **196** (7) 708 – 725 (2026)
Translated by the authors

* This review is based on the report presented for the Scientific Session of the Physical Sciences Division of the Russian Academy of Sciences (PSD RAS), on May 21, 2025 (see *Physics–Uspekhi* **69** (7) 663 (2026); *Uspekhi Fizicheskikh Nauk* **196** (7) 707 (2026)).

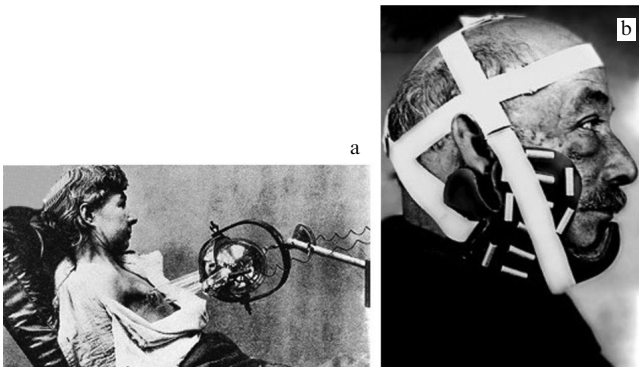

Figure 1. (a) Irradiation of the breast (E.H. Grubbe, 1896). (b) Treatment of skin cancer with radium (Curie Institute, 1922).

In 1921, physicists developed the first ionizing-radiation detectors, namely ionization chambers. The first dosimetric unit, the roentgen, was introduced in 1928 and allowed dose measurements to be standardized. During the 1930s, physicists calculated the first dose tables for estimating the dose absorbed by biological tissue. In addition to maintaining equipment, physicists in medical institutions were assigned responsibility for dose calculations in diagnostic and therapeutic procedures in order to reduce recurrence rates. This reduced the incidence of complications. Specialists who performed this work came to be known as medical physicists. They became part of clinical teams responsible for calculating treatment schedules and for monitoring equipment safety and performance [10, 11].

Radiation protection developed in parallel: the first limits on occupational and patient doses began to be introduced in the 1930s [12].

In 1942, Yale University pharmacologist L. Goodman proposed using the chemical-warfare agent nitrogen mustard to arrest tumor growth. The first experiment in which this poison was used to treat lymphosarcoma produced a favorable result [13] and foreshadowed the development of chemotherapy.

By the middle of the twentieth century, cancer treatment was gradually taking the form of a combination of surgery, chemotherapy, and radiotherapy. This laid the foundation for the modern oncological triad, in which the three modalities are regarded as complementary. Medical physicists play a central role in optimizing radiotherapy, ensuring its safety, and controlling the quality of the treatment process [12, 14]. This field is now referred to as radiation medical physics and encompasses radiotherapy, diagnostic imaging, and radionuclide diagnosis and therapy. [1]

In Russia, the term medical physics covers both the operation of medical equipment and the development of new equipment and technologies for medicine. Its scope is therefore substantially broader than that generally adopted by the international community. The instruments, systems, and methods created for medicine by physicists from different disciplines can be divided broadly into those that use ionizing radiation and those that use nonionizing radiation (Fig. 2). The numbers of medical systems in these two categories are approximately equal worldwide. In total, approximately 10 million high-technology medical devices and systems are in use. They include ultrasound systems, lasers, electromagnetic-therapy devices, different types of imaging systems — magnetic resonance imaging (MRI), X-ray computed tomography (CT), single-photon emission computed tomography (SPECT), and positron emission tomography (PET) — linear and circular accelerators for electrons, protons, and ions, and isotope-based devices and instruments.

[1] Radionuclide diagnosis and therapy are usually grouped together under the term nuclear medicine in international practice.

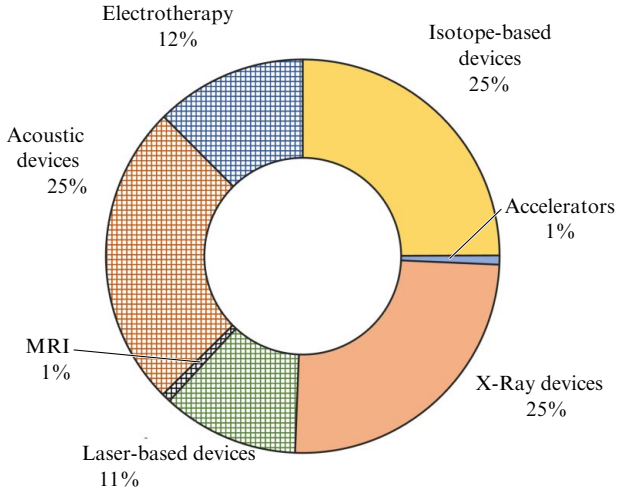

Figure 2. Medical devices and systems that use ionizing and nonionizing radiation.

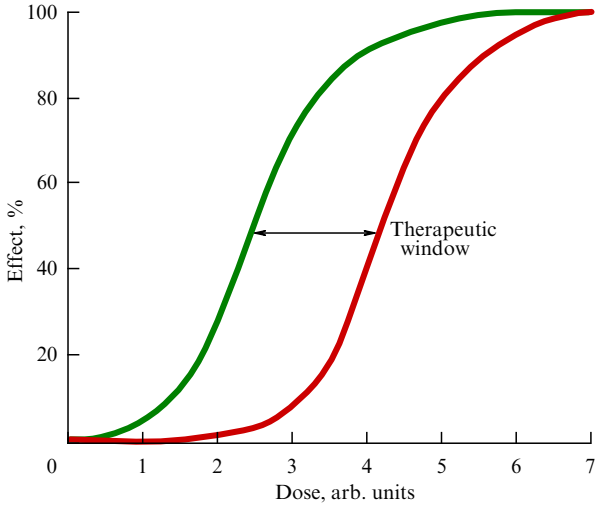

Figure 3. The therapeutic window.

This review focuses on the mechanisms by which ionizing radiation produced by radiation-generating systems, instruments, and devices acts on biological tissue.

Experiments have shown that, within certain dose ranges, malignant cells die more rapidly than normal cells even when both receive the same dose [15]. This difference arises because normal tissues are more capable of recovering from radiation damage. The difference between doses that destroy tumor cells and those that can be tolerated by normal tissue is termed the therapeutic window (Fig. 3).

The width of this window varies with tissue and organ type. Radiotherapy seeks to concentrate as much of the radiation dose as possible in the tumor while minimizing the dose to surrounding normal tissue. This approach widens the therapeutic window and improves treatment efficacy.

This fundamental radiobiological finding is associated with a series of studies by L.H. Gray, R.M. Sievert, and other scientists.

In 1926, J.A. Crowther established that rapidly dividing cells, such as tumor, epithelial, and bone-marrow cells, are damaged more severely than slowly renewing tissues such as muscle and nerves [16].

In 1936, the English physicist L.H. Gray found that tissue oxygenation increases radiation damage. This oxygen effect improves the efficacy of radiotherapy.

The Swedish physicist R.M. Sievert developed methods for measuring absorbed radiation dose and introduced the concept of equivalent dose, measured in sieverts (Sv) [17]. His work allowed the effects of radiation on different tissues to be assessed more accurately and subsequently helped define the range of doses that maximizes tumor-cell damage while minimizing injury to normal tissue.

In 1946, D.E. Lea introduced the concept of lethal chromosomal lesions per gray [18]. These data formed the basis of R. Paterson's 1948 classification of tumors by radiosensitivity.

In 1944, H. Coutard proposed fractionated irradiation, in which multiple small doses are delivered instead of a single large dose [19]. Fractionation allows normal tissue to recover between sessions while tumor cells accumulate more damage. Dividing the total dose into many sessions, or fractions, increases tumor damage as cells redistribute into radiosensitive phases of the cell cycle and gives normal tissue time to recover. For example, a single dose of 20 Gy may cause skin necrosis, whereas 30 fractions of 2 Gy, for a total dose of 60 Gy, are safer and more effective.

The concepts of the therapeutic window and therapeutic ratio were introduced in the 1960s on the basis of the accumulated radiobiological evidence.

The therapeutic window (Fig. 3) defines the limits within which radiation can be used safely. Its lower boundary is the minimum dose required to destroy the tumor, and its upper boundary is the maximum dose that normal tissue can tolerate without irreversible damage. It is, in effect, the dose range within which treatment is possible [20].

The therapeutic ratio (TR) is a numerical measure of the extent to which radiation destroys the tumor relative to the damage it causes to normal tissue:

$$\mathrm{TR} = \frac{\text{Tumorcell death}}{\text{Damage to normal tissue}}\,.$$

The higher the TR, the more effective the treatment. An optimal treatment maximizes tumor-cell destruction while minimizing damage to normal tissue.

A broad therapeutic window usually makes it easier to achieve a high TR because it provides greater scope for selecting an effective and safe dose. Methods that increase the TR, such as precise beam focusing, may therefore widen the therapeutic window in an individual case.

The therapeutic ratio is a central concept in radiation oncology because it quantifies the efficacy and safety of radiotherapy. It represents the balance between tumor-cell killing and normal-tissue damage.

As noted above, industrial production of radiotherapy and X-ray equipment and radionuclide sources began in the 1930s [11], when the first attempts were also made to use particle accelerators in medicine. At this time, physicists and physicians began to work together in clinical practice,

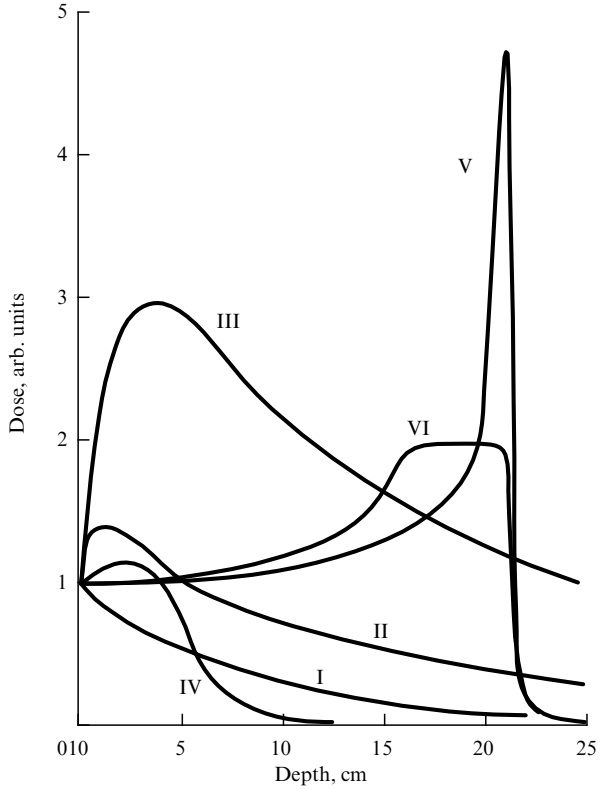

Figure 4. Dose as a function of penetration depth in tissue for (I) 200-kV X-rays, (II) radiation from ^{60}Co, (III) 22-MeV high-energy photons, (IV) 22-MeV electrons, (V) 200-MeV protons, and (VI) a spread-out Bragg peak.

establishing the organizational and methodological foundations of medical physics as an independent scientific and practical field. Radiation medicine became interdisciplinary, with physicists and clinicians jointly developing diagnostic and therapeutic methods. This collaboration improved treatment efficacy and substantially reduced the incidence of severe complications by standardizing doses and advancing quality control [10, 12]. Equipment, dosimetry methods, and treatment-planning procedures were also progressively improved [11, 12, 14].

Table 1 summarizes the principal milestones in the development of radiation medical physics, highlights important advances in physics, and indicates the contribution of medical physicists at each stage. Progress in physics determined the development of cancer diagnosis and treatment. X-ray, nuclear, computed-tomography, and magnetic-resonance imaging made noninvasive tumor detection possible, while advances in dosimetry and accelerator technology enabled precise, individualized radiotherapy. Physicists developed the foundations of dosimetric treatment planning and methods for calculating and verifying energy distributions, thereby improving the safety and efficacy of cancer treatment.

Figure 4 shows depth-dose distributions for different types of radiation: X-rays (I), cobalt-60 gamma radiation (II), high-energy bremsstrahlung photons (III), electrons (IV), the Bragg peaks of protons and ions (V), and a spread-out Bragg peak (VI) [49].

The underlying principle is straightforward: cells die when ionization events occur within them. Cancer cells divide more rapidly and are therefore killed at lower doses than normal

Table 1. Major milestones in the development of radiation medical physics and the contribution of medical physicists at each stage.

Year(s)	Event	Impact on medicine and clinical practice
1895	Discovery of X-rays [1]	Emergence of diagnostic radiology
1896	Discovery of radioactivity [2]	Introduction of radionuclides into medicine
1896	First use of X-ray therapy [21]	Beginning of the therapeutic use of radiation
1898–1902	Discovery of polonium and radium; studies of radioactivity [4]	Introduction of isotopes into medicine
1903	Use of radionuclides to treat carcinoma in Russia [22]	Emergence of brachytherapy
1918	Establishment of the State Institute of Roentgenology and Radiology [23]	Foundation of the Russian school of radiology
1921	Development of the first ionization chamber [24]	Introduction of a method for measuring dose
1922	Production of the first Russian radium preparation [25]	Beginning of domestic isotope production
1928	Introduction of the roentgen as a unit [26]	Emergence of dosimetry in clinical practice
1930s	Emergence of radiobiology [27, 28]	Characterization of tumor radioresistance
1930s	Physicists begin working in hospitals [29, 30]	Improvement in treatment quality
1934	Introduction of fractionated irradiation [30]	Development of dose-fractionation standards
1937	First medical electron accelerator, London [31]	Introduction of accelerators into medicine
1946	Emergence of nuclear medicine [32]	Large-scale production of isotopes for medicine
1949	Development of the gamma camera [33]	Use of isotopes for imaging
1950	First Soviet medical electron linear accelerator [34]	Development of domestic medical technology
1951	Development of cobalt therapy units [35]	Wider availability of external-beam radiotherapy
1954	First use of a proton accelerator in medicine [36–38]	Introduction of proton therapy
1954–1955	First clinical trials of boron neutron capture therapy using reactor neutrons [39]	Beginning of clinical testing of the method
1960s	Concept of the therapeutic window [40]	Improvement in treatment efficacy
1971	Development of the CT scanner by Hounsfield [41, 42]	Three-dimensional imaging of internal organs
1968	First Gamma Knife unit [43]	Treatment of brain tumors without open surgery
1973	First MRI systems [44, 45]	Application of physical and chemical magnetic-resonance techniques
1980–1990s	Emergence of computerized dosimetric treatment planning [46, 47]	Introduction of individualized radiotherapy plans
2010s	Development of the Russian ONYX and Brachium systems	Domestic production of medical equipment
2014	Emergence of FLASH radiotherapy [48]	Delivery of ultrahigh dose rates to tumors

cells. Irradiation must be delivered in a way that widens the therapeutic window and increases the probability of eliminating tumor cells. Each type of ionizing radiation has its own range of applications; none can be described as categorically unsuitable for radiotherapy. Approximately 300 types of tumors are known. Each type of radiation is effective against a particular set of tumors and less effective against others.

For a 200-kV X-ray beam, the maximum dose occurs at the surface, in the skin. The photons emitted by ^{60}Co have a mean energy of 1.25 MeV, and the dose maximum lies close to the surface, at a depth of approximately 0.5 cm. Electron beams have dose maxima at depths of approximately $\sim$ 2.5–7 cm and are likewise used to irradiate relatively superficial tumors. Deep-seated tumors at depths of approximately $\sim$ 10–30 cm are treated with bremsstrahlung photon, proton, or ion beams. A major advantage of protons, for example, is their ability to treat deep-seated tumors of virtually any shape and location without substantial damage to surrounding tissue [50–52]. Cobalt units were also widely used in the past, but experience showed that they could cause substantial radiation injury to superficial tissues.

The central objective of radiation medical physics is to deliver most of the dose to the tumor and as little as possible to normal tissue. Tumors therefore began to be irradiated from multiple directions using bremsstrahlung photon, proton, and ion beams. The idea of optimizing dose delivery to maximize tumor control while minimizing normal-tissue damage was formulated in the work of Claude Regaud and Henri Coutard in the 1920s and 1930s.

This arrangement markedly improves the ratio of tumor dose to normal-tissue dose (Fig. 5) and is known as conformal radiotherapy. To implement it, physicists developed complex mechanical systems known as gantries. A gantry rotates through 360 degrees around the patient and allows the beam to be delivered from any angle (Fig. 5). Many additional technical and computational methods have since been developed to align the treatment plan with the tumor as closely as possible.

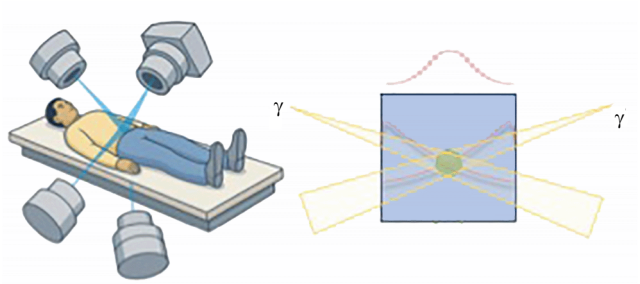

Figure 5. Conformal radiotherapy: schematic irradiation of a tumor with bremsstrahlung photon beams delivered from different directions.

2. Methods for improving the efficacy of radiotherapy and diagnostic imaging

In the 1930s, only approximately 5% of treated cancer patients survived for more than five years. This proportion increased to 30–40% in the 1960s and now exceeds 70%. This progress reflects the effective combination of surgery, chemotherapy, and methods based on radiation medical physics.

The main aim of therapy is to prolong a patient's life or achieve a complete cure. Over the past decade, many patients have survived for 10–25 years after radiotherapy. As survival has improved, clinicians have increasingly encountered late treatment effects [53], which may appear 10–15 years after therapy. These include recurrences and secondary malignancies. Recurrences may result from an insufficient tumor dose [54], whereas secondary malignancies may arise from excessive irradiation of normal tissue [55]. Their development can also be affected by many other medical, physical, and chemical factors [53]. Our studies focus on the role of physical factors in adverse effects following radiotherapy.

Reference [56] presents a comprehensive study of uncertainties in the physical factors associated with diagnostic imaging and radiotherapy. In some cases, these uncertainties may contribute to post-radiation or secondary cancers (Fig. 6).

2.1 Uncertainties in the physical factors of diagnostic imaging and radiotherapy

Studies [57, 58] indicate that up to 80% of secondary malignancies are associated with irradiation received during radiotherapy. Our group has experimentally investigated several physical factors that generate unaccounted-for doses using medical electron accelerators at different oncology centers.

The physical uncertainties encountered during a course of radiotherapy can be divided into three categories: uncertainties associated with preparing the patient for treatment, unaccounted-for doses arising during treatment planning, and uncertainties in the actual delivery of the prescribed dose. Each category may substantially affect the dose received by the patient and, consequently, the outcome of treatment, including recurrence and adverse effects. These uncertainties also increase the risk of secondary tumors.

Uncertainties in diagnostic imaging. These arise in CT and MRI as well as in emission tomography, including PET and SPECT. The choice and use of imaging methods can substantially affect treatment outcomes [59] and have therefore been studied extensively.

Computed tomography. CT is the principal imaging method used for diagnosis and radiotherapy planning. A single CT examination typically adds 10–30 mGy [60]. When multiple scans are performed for follow-up or replanning, the cumulative dose may reach 100–250 mGy [61, 62]. Reference [59] shows that frequent CT examinations, for example during surveillance of patients with early gastric cancer, increase the risk of malignant cell transformation. In a study of patients with different malignant tumors [63], an increase in the number of CT examinations was associated with a 15% rise in the risk of secondary cancers.

Positron emission tomography. PET/CT improves diagnostic accuracy and the assessment of treatment response, but it also increases radiation exposure and the risk of secondary carcinogenesis. In [64], the combined effective dose from PET and CT ranged from 66 to 113 mGy in children and was approximately 97 mGy in adults. This exposure increases the risk of radiation-induced disease, particularly in younger patients.

Single-photon emission computed tomography. SPECT/CT used in the diagnosis of thyroid cancer also produces an unaccounted-for radiation exposure. A single examination typically delivers 10–20 mGy [65], and the dose accumulates when serial examinations are performed. Reference [66] demonstrates the need to minimize additional diagnostic procedures. At the same time, post-therapy SPECT/CT can

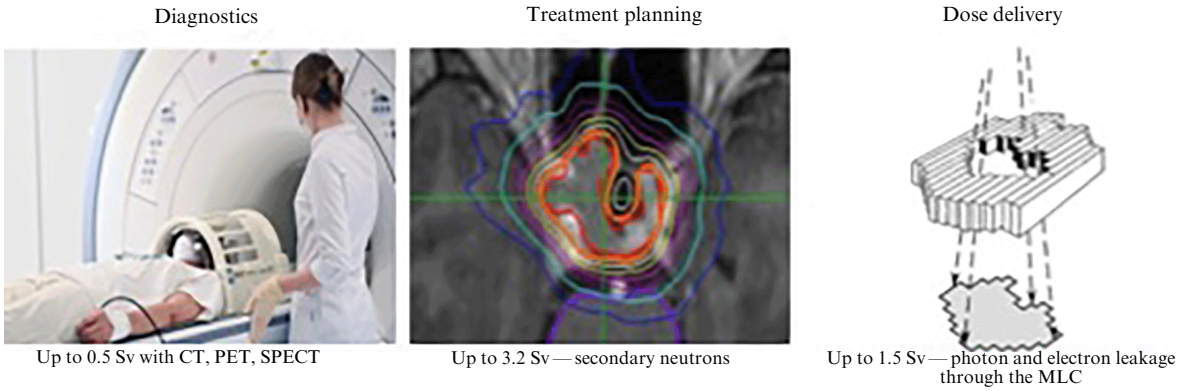

Figure 6. Estimated unaccounted-for doses at all stages of radiotherapy [56]: diagnostic procedures, up to 0.5 Sv from CT, PET, and SPECT; treatment planning, up to 3.2 Sv from secondary neutrons; and dose delivery, up to 1.5 Sv from photon and electron leakage through a multileaf collimator.

reduce the number of additional examinations in approximately 20% of patients and may reduce the probability of recurrence in 6.4% [67].

Studies [68–71] have shown that the probability of secondary malignancy after PET and SPECT depends on patient age and disease type. These examinations are also susceptible to false-positive results [72], which occur in 20–40% of patients [73]. False-positive findings prompt additional examinations and increase radiation exposure. Repeated investigations may add tens of milligrays and, in some cases, 50–100 mGy [74, 75].

The effects of low-dose radiation vary with genetic susceptibility and patient age, indicating that existing risk models require further improvement. CT, PET, and SPECT examinations performed in preparation for radiotherapy planning may together produce approximately 0.5 Gy of unaccounted-for dose.

Magnetic resonance imaging. MRI is widely used in radiotherapy planning, particularly for tumors of the brain and prostate. It provides high soft-tissue contrast and improves the accuracy with which target boundaries are defined. MRI also avoids ionizing radiation, which is important for reducing the risk of secondary tumors. Nevertheless, geometric distortions in MR images can produce errors in the positions assigned to the target and organs at risk. These errors may reduce the accuracy of dose delivery and expose normal tissue to an unaccounted-for dose.

In our study [76] using a Tomikon S50 0.5-T scanner and a Siemens Magnetom Avanto 1.5-T scanner, the maximum coordinate displacement reached 5 mm at a distance of 160 mm from the magnet isocenter, while the mean displacement was approximately 2.5 mm. The magnetic-field gradient was calculated to assess the distortion, and coordinate displacement was found to increase linearly with the gradient. With the 0.5-T MRI system, the error in the measured area of a 1.5-cm-diameter object reached 28%. A distortion of this magnitude may expose normal tissue to an additional dose of up to 1.6 Gy and cause underdosage of the tumor.

A 1-mm displacement of a tumor in an MR image can reduce dose coverage of small objects with a volume of 0.1 cm^3 by as much as 13%, corresponding to an underdose of 0.9 Gy. At displacements of 2–3 mm, the dose deficit reaches 30%, which is roughly equivalent to a loss of up to 2.1 Gy. For objects larger than 5 cm^3, the reduction in coverage for the same displacements is no greater than 3%, corresponding to a dose error of approximately 0.7 Gy.

Our results agree well with other studies. References [77–80] report positional deviations of up to 5 mm at a distance of 160 mm from the magnet isocenter, with the largest deviations observed for rapid gradient-echo sequences.

Taken together, geometric distortion and displacement in MRI-based planning may expose normal tissue to additional radiation and reduce the tumor dose by as much as 2–2.5 Gy over a treatment course.

Uncertainties in radiotherapy planning. During treatment planning, unaccounted-for doses arise mainly from nuclear reactions. Interactions of proton and bremsstrahlung photon beams with accelerator components and the patient's tissues generate secondary photons, electrons, and neutrons.

Secondary neutrons are produced above the threshold for photonuclear reactions, approximately 10 MeV. In our study [81], the spectra of secondary neutrons generated by medical electron linear accelerators were measured experimentally. The measurements were performed on Varian, Siemens, and Elekta accelerators. A DSN-01 spectrometer based on the Bonner-sphere method with an activation tantalum target was used to measure the secondary-neutron spectra. The experiments employed photon-beam energies of 15–20 MeV and field sizes of up to 40×40 cm^2. The mean neutron energy obtained from the reconstructed spectrum was 0.89 MeV for a 20-MeV electron beam.

In our studies [56, 82], the contribution of secondary neutrons to the additional dose was estimated by numerical simulations performed with Geant4. We calculated the local dose deposited in a thin water layer inside a water phantom as bremsstrahlung interacted with accelerator components and the surrounding environment. The simulations showed that neutrons generally contributed no more than 0.2–0.4% of the absorbed dose in this local volume.

In another of our studies [83], a broader approach was used in which the parameters were averaged over different field sizes, depths, and energies up to 20 MeV; the neutron contribution was 1.5%. The out-of-field dose was found to reach 2–4%.

Our results [56, 81–83] agree with other published findings. References [84–86] show that the neutron contribution to dose, particularly at high energies, substantially increases the risk of secondary tumors, and that the total additional dose accumulated during fractionated irradiation may exceed the dose from a single treatment fraction. Uncertainties related to the equipment and the patient's condition increase the unaccounted-for dose by a further 5% [87, 88].

For a conventional treatment delivering 70 Gy in 35 fractions, the total dose from secondary particles may reach 3.2 Gy, nearly equivalent to the dose delivered in two treatment fractions.

Uncertainties in dose delivery. The accuracy of dose delivery during radiotherapy is affected by uncertainties associated with equipment performance, patient positioning, and organ motion [88]. Studies [89, 90] report that errors in the accelerator collimation system can displace the beam by 2–3 mm. References [87, 91] show that motion of the patient's organs relative to their positions in the original plan produces dose-delivery errors of 1–2%. For a complete treatment course with a total dose of 70 Gy, these errors may increase the dose not accounted for in the treatment plan by up to 1.4 Gy [92].

Multileaf collimators are installed in the beam path within the heads of medical linear accelerators. A multileaf collimator consists of many narrow metal leaves that move independently, allowing the irradiation field to conform closely to the shape of the tumor. Its principal purpose is to reduce the dose to surrounding normal tissue. Some radiation nevertheless passes through gaps between the leaves and creates an additional dose outside the tumor. In our studies [82, 93], we estimated unaccounted-for doses outside the treatment field and found that they may reach 1.5 Gy over a course of treatment.

A comprehensive analysis of the physical factors that affect dose distributions in radiotherapy allowed us to estimate an upper bound for the total unaccounted-for dose to normal tissues and the central nervous system. The individual contributions are approximately 0.5 Gy from diagnostic procedures, up to approximately 2.5 Gy from MRI distortion during planning, up to approximately 3.2 Gy from secondary neutrons during treatment with bremsstrah-

lung photon beams, approximately 1.5 Gy from particle leakage through the MLC, and approximately 1.4 Gy from motion of internal organs relative to the treatment plan. If all of these adverse factors coincide — for example, MRI-based planning for a brain tumor, treatment with bremsstrahlung photons using an MLC, and several CT, PET, or SPECT examinations before treatment — the maximum unaccounted-for dose may reach approximately 9 Gy over the treatment course.

Unaccounted-for doses can cause both immediate and late effects [15]. Numerous models for estimating the risk of secondary malignancies have been developed from statistical data and large epidemiological studies. The risk of secondary brain tumors, including meningioma and glioma, can be estimated using the standard linear model presented in [94]. In this model, the excess relative risk (ERR) of a radiation-induced tumor increases in proportion to the cumulative dose:

$$\mathrm{ERR} = kD\,.$$

The coefficient k is taken to be 0.56 for adults [95, 96] and 1.06 for children [97]. Thus, each additional gray increases the ERR of a secondary tumor by 0.53 in adults and 1.06 in children relative to an unexposed individual.

At the upper estimate of 9 Gy for the unaccounted-for dose, the ERR in an adult is approximately 4.8, corresponding to a total risk approximately 5.8 times that in an unexposed individual. The lifetime risk of a brain tumor in the unexposed population is 1%, or 10 cases per 1000 people. Exposure to the estimated unaccounted-for dose therefore raises the absolute risk to 5.8%, or 58 cases per 1000 patients. In young patients, including children and adolescents, the excess relative risk is higher, reaching approximately 9.5, and the absolute risk rises to approximately 10%, or 100 cases per 1000 patients.

The risk of secondary tumors therefore increases substantially as unaccounted-for dose accumulates. This finding emphasizes the need to control and minimize every source of uncertainty during radiotherapy planning and delivery.

2.2 Uncertainties in diffusion-weighted magnetic resonance imaging

Radiotherapy is often the most effective treatment for brain tumors because it does not require surgery. To irradiate a tumor with a photon beam without damaging normal tissue, clinicians must be able to identify the tumor boundaries and the locations of critical structures such as the optic nerve. Conventional MRI and CT show the general anatomy, but the boundaries between tumor, normal tissue, and treatment-related edema are often blurred. It may therefore be difficult to determine where the tumor ends and normal tissue and nerve fibers begin.

Physicists developed diffusion-weighted imaging (DWI) to address this problem. The method measures diffusion, that is, the motion of water molecules in tissue [98].

A diffusion tensor **D** is constructed in every elementary volume of the region under investigation (Fig. 7). The resulting data are used to build a mathematical model of water-molecule motion in the tissue.

Diffusion in biological tissue is described by a symmetric positive-definite tensor **D**, which can be written as

$$\mathbf{D} = p\mathbf{I} + \mathbf{Q}\,.$$

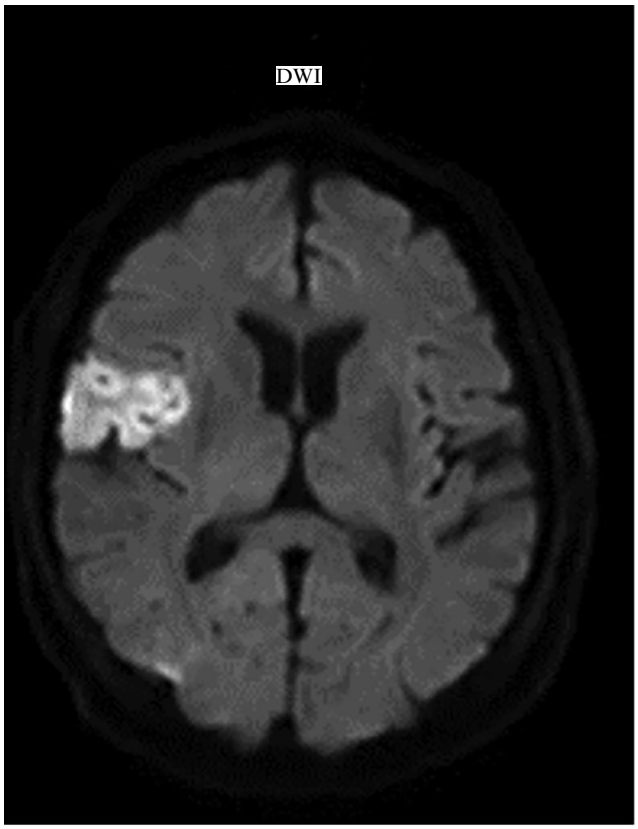

Figure 7. Example of a diffusion-weighted image.

Here, p is the isotropic component, which represents random, nondirectional motion of water molecules and is associated with tumor infiltration into adjacent tissue; **I** is the identity matrix; and **Q** is the anisotropic component, which describes directional diffusion and is associated with volumetric tumor growth.

Processing of MR images yields the eigenvalues λ_i ($i = 1, 2, 3$) of **D**. The diffusion tensor is a symmetric 3×3 matrix:

$$\mathbf{D} = \begin{matrix} D_{xx} & D_{yx} & D_{zx} \\ D_{xy} & D_{yy} & D_{zy} \\ D_{xz} & D_{yz} & D_{zz} \end{matrix}\,. \tag{1}$$

The diagonal elements (D_{xx}, D_{yy}, and D_{zz}) describe diffusion along the x, y, and z axes. The trace ($\mathrm{Tr}\,(\mathbf{D})$) is the sum of the diagonal elements:

$$\mathrm{Tr}\,(\mathbf{D}) = D_{xx} + D_{yy} + D_{zz}\,. \tag{2}$$

Diagonalization of the tensor gives eigenvalues that describe diffusion along the principal directions. The trace is also equal to the sum of the eigenvalues:

$$\mathrm{Tr}\,(\mathbf{D}) = \lambda_1 + \lambda_2 + \lambda_3\,. \tag{3}$$

The mean diffusivity (MD) is the arithmetic mean of the eigenvalues, or equivalently of the diagonal elements, and characterizes the *overall mean-square displacement of the molecules*:

$$\mathrm{MD} = \frac{\mathrm{Tr}\,(\mathbf{D})}{3} = \frac{(\lambda_1 + \lambda_2 + \lambda_3)}{3} = \frac{(D_{xx} + D_{yy} + D_{zz})}{3}\,. \tag{4}$$

The isotropic part (p) of **D** characterizes the overall level of diffusion and correlates with the ability of a tumor to invade surrounding tissues and organs. A higher value of p indicates more disordered molecular motion and may therefore indicate a more aggressive tumor. It is obtained from the mean diffusivity:

$$p = \sqrt{3}\mathrm{MD}\,, \tag{5}$$

The anisotropic part (q) reflects directional tumor growth along fibers or vessels and is associated with volumetric expansion. It is determined from the differences between the eigenvalues:

$$q = \sqrt{(\lambda_1 - \mathrm{MD})^2 + (\lambda_2 - \mathrm{MD})^2 + (\lambda_3 - \mathrm{MD})^2}\,. \tag{6}$$

The parameters p and q make it possible to identify not only the main tumor volume but also a target volume that includes the presumed spread of tumor cells into neighboring tissues.

Water molecules move differently in different tissues. In cerebrospinal fluid they move freely and randomly, producing isotropic diffusion. In nerve fibers, water moves predominantly along the fiber direction because cell membranes restrict transverse motion, producing anisotropic diffusion. When water molecules move freely, as in a fluid or edema, the signal decreases. The denser the medium, the more restricted the molecular motion, the sharper the boundary, and the brighter the signal in the image. Tumors therefore appear brighter than other tissues.

DWI is currently used to detect acute stroke, in which the ischemic region appears bright; to diagnose and monitor tumors, where denser tissue produces a stronger signal; and to detect inflammation and abscesses.

A more advanced form of diffusion-weighted imaging, diffusion tensor imaging (DTI), was subsequently developed. DTI determines not only whether diffusion is restricted but also the direction in which the restriction occurs. Its mathematical model constructs the diffusion tensor in three spatial dimensions. DWI shows the tumor itself, whereas DTI shows how a nerve tract passes around it and can therefore help a clinician avoid damaging structures such as the optic nerve. The principal diffusion direction coincides with the orientation of nerve fibers. Color maps are used for three-dimensional visualization (Fig. 8): red indicates fibers running right to left, such as the corpus callosum; green indicates fibers running anterior to posterior, such as the pyramidal tracts;[2] and blue indicates fibers running superior to inferior, such as the corticospinal tracts.[3]

DTI is now used to plan surgery and radiotherapy so that important tracts can be spared, to assess the effects of trauma such as fiber disruption after traumatic brain injury, and to study neurodegenerative diseases such as multiple sclerosis.

These methods have been used to develop the first Russian software product for preprocessing, processing, visualization, and analysis of DWI data that can be integrated into a radiotherapy treatment-planning system (Fig. 9).

In Figure 9, the initial region is outlined in green. Mathematical processing of the MR image by the proposed methods showed that the actual tumor volume, outlined in red, was smaller than originally assumed. This approach improves the accuracy with which the high-dose irradiation volume is defined and reduces the dose to normal tissue by an average of 30–40% [99]. This reduction is particularly important for limiting radiation injury to normal tissue and preserving the option of reirradiation if the tumor recurs, thereby improving long-term prognosis. Minimizing normal-tissue irradiation also reduces the risk of secondary malignancies, which is an important advantage of the method.

[2] The pyramidal tracts, also known as the pyramidal pathway or corticospinal tract, are a system of nerve fibers connecting the motor centers of the cerebral cortex with the motor nuclei of the cranial nerves and the cells of the anterior horns of the spinal cord. They mediate voluntary movement.

[3] The corticospinal tract is a motor pathway in the white matter. Its principal function is voluntary motor control of the trunk and limbs.

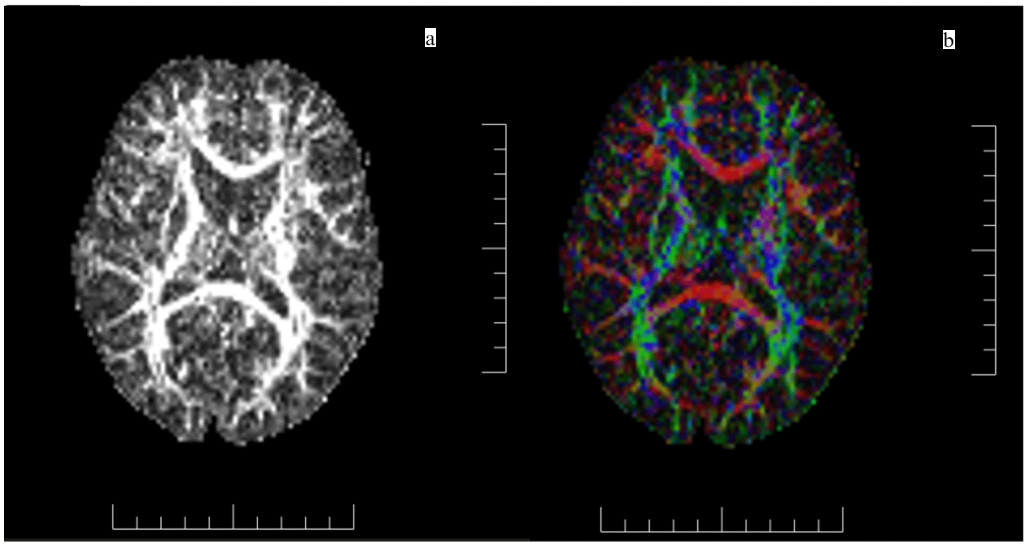

Figure 8. Example of diffusion tensor imaging: (a) distribution of fractional anisotropy (FA), which indicates how strongly diffusion differs among directions; (b) color-coded FA distribution.

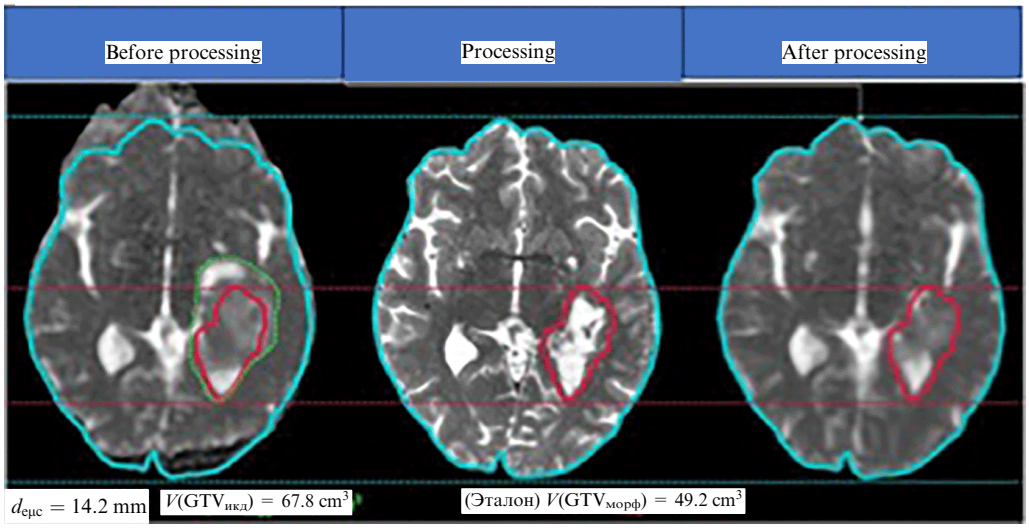

Figure 9. Example of MR-image processing for radiotherapy of a brain tumor.

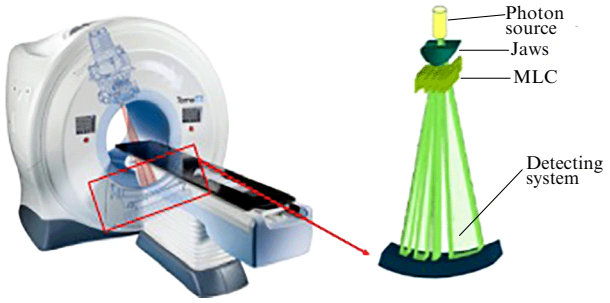

Figure 10. Use of data from all detectors built into the TomoTherapy system to monitor patient irradiation over the course of treatment [100].

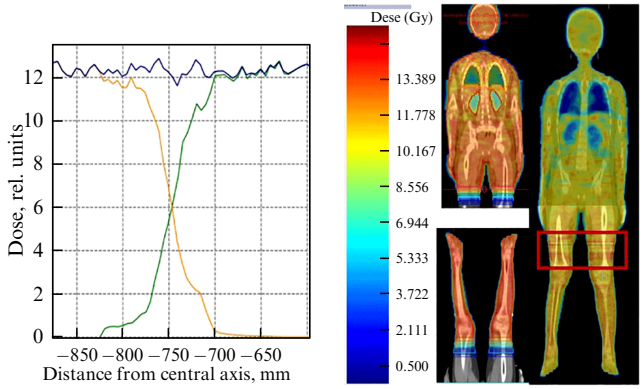

Figure 11. Conformal total-body irradiation by helical tomotherapy [100].

2.3 Transit dosimetry using detectors built into the TomoTherapy system

In collaboration with the Dmitry Rogachev National Medical Research Center, we developed a method for improving radiotherapy quality by using data from all detectors built into the TomoTherapy system to monitor patient irradiation throughout treatment.

The principle is as follows. TomoTherapy is a unique accelerator-based treatment system. It resembles a CT scanner, but the X-ray tube is replaced by a compact 6-MeV accelerator. As the treatment couch moves through the system, the patient is irradiated helically. The detector array shown as a black arc in Fig. 10 is used to position the patient according to the treatment plan. Ordinarily, its data are used only during patient setup. We developed a software package[4] that also uses these data during irradiation. It enables continuous monitoring of system performance and of the accuracy with which the tumor is irradiated, substantially extending the capabilities of the system.

2.4 A method for irradiating large tumors with TomoTherapy and Elekta Synergy accelerators

TomoTherapy systems are among the most advanced radiotherapy units currently available. Their worldwide number is relatively small, approximately 400, and only three operate in Russia. In collaboration with the Dmitry Rogachev Center, we developed an innovative method that is now used both in Russia and abroad. The method is implemented on TomoTherapy and Elekta Synergy linear accelerators and uses intensity modulation to deliver conformal irradiation to extended tumors more than 1–1.5 m in length.

By matching treatment plans for different parts of the body, the method can irradiate both large tumors and the entire body. Total-body irradiation is particularly important in conditioning pediatric patients for bone-marrow transplantation. A single treatment plan cannot cover a person's full height when it exceeds approximately 1.5 m.

The main difficulty in irradiating large targets is the limited field size of the accelerator, which makes field-junction regions necessary. Because the accelerator aperture does not cover the patient's entire body, two and sometimes three treatment plans must be matched. Their dose distributions must be joined without creating an underdosed or overdosed region. Dose does not fall to zero instantaneously but over a finite spatial interval. Figure 11 shows the dose distributions in the plan-junction region for two parts of the body, represented by the orange and green curves. A suitable intersection point must be selected. We developed a method for choosing this point and verified it by gamma-index analysis and Geant4 simulations [100]. The resulting dose distribution is uniform across the plan junction, as shown by the blue curve in Fig. 11.

Underdosage may lead to recurrence, whereas overdosage increases the probability of secondary cancers. The method

[4] The software package has been registered as intellectual property.

produces a highly uniform dose distribution in the overlap region, minimizes the dose to critical organs while maintaining the therapeutic target dose, and allows dosimetric uncertainties to be estimated so that underdosage and overdosage can be prevented.

The method developed jointly by Moscow State University and the oncology center is used in clinical practice. It has been applied to 600 children aged 10–16 years with leukemia and large tumors. Seven years of follow-up have yielded favorable outcomes. The method has therefore been incorporated into clinical guidelines issued by the Ministry of Health of the Russian Federation and is also used in the United States, the European Union, and other countries.

2.5 Physical and technical studies for synchrotron-based proton radiotherapy

Proton radiography system. The Protvino Branch of the Lebedev Physical Institute, under the leadership of Corresponding Member of the Russian Academy of Sciences V.E. Balakin, developed the first Russian medical proton accelerators based on proton synchrotrons. Their energy is variable from 70 to 250 MeV, the proton-beam intensity is 10^9 s^{-1}, the outer diameter is 5 m, and acceleration to the maximum energy takes 1 s. Figure 12a shows the accelerator.

Working with staff of the Protvino Branch, including postgraduate students from our department who were also employed at the medical synchrotron, we addressed two important problems.

First, we developed a Russian proton-radiography system. Anatomical imaging is ordinarily performed using CT. We proposed operating the proton beam in two modes: a high-intensity therapeutic mode and a low-intensity diagnostic mode for proton radiography. The wide range straggling of the protons required dedicated correction algorithms. The low-intensity proton beam was then used to image the irradiated part of the body, such as the head shown in Fig. 12b.

Low-intensity proton imaging visualizes the patient's anatomy without delivering an unnecessary dose. A domestic proton-radiography system was thus developed for the Russian medical synchrotron [102].

The second task was to develop a respiratory — motion management system for the same accelerator.

Comparable methods for radiotherapy with bremsstrahlung photon and electron beams are well established and have proved effective. Figure 13 shows the motion of a tumor, visible as a bright region, relative to the treatment field indicated by the lines with arrows. Proton pulses are delivered when the beam position is synchronized with the tumor motion, generally at full inspiration.

Compensating for tumor motion during synchrotron irradiation is difficult because the particles undergo several stages of acceleration. In the conventional operating mode, the beam is accelerated and stored in the ring until an extraction trigger is received. This leads to particle losses of up to 50% over 10 s, incomplete irradiation, and magnet overheating.

We therefore proposed a new approach (Fig. 14) that controls both particle extraction and injection. It predicts when acceleration must begin so that the beam is ready for extraction at precisely the required time. The approach eliminates idle storage, ensures complete irradiation, and reduces the load on the magnetic system [103].

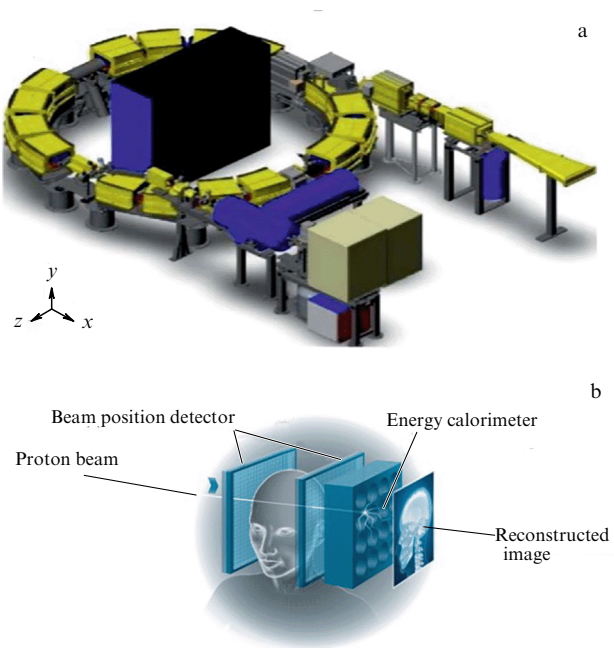

Figure 12. (a) The Russian Prometheus proton synchrotron at the Lebedev Physical Institute, Protvino. (b) Schematic of proton radiography during irradiation of a brain tumor [101].

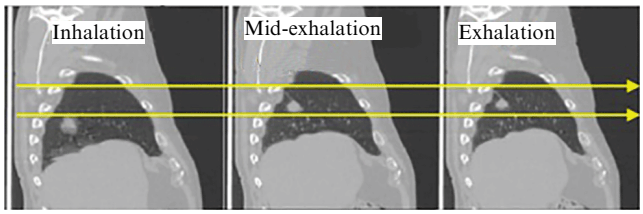

Figure 13. Frontal CT projections of a patient with a lung tumor at three phases of respiration: inspiration, mid-expiration, and expiration. The images show tumor motion. In this clinical case, the maximum tumor displacement in the superior-inferior direction was 31 mm [101].

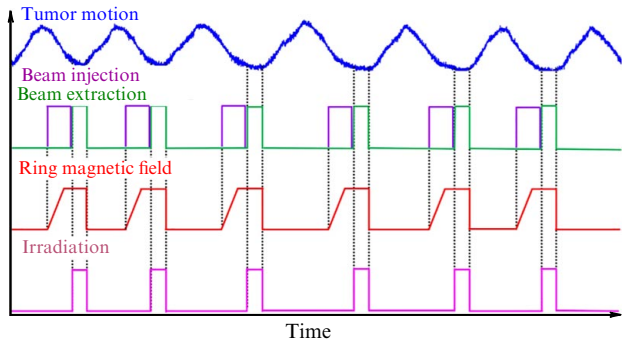

Figure 14. Timing diagram of the new synchrotron irradiation mode for a moving tumor.

2.6 Production of radionuclides for nuclear medicine using electron accelerators

Modern nuclear medicine uses approximately 45 radionuclides, including 37 for diagnosis and 27 for therapy. They are incorporated into radiopharmaceuticals that are administered to the patient. Each radionuclide has a characteristic biodistribution and may accumulate in tumor tissue within particular organs. The isotopes decay by emitting photons, electrons, or ions. A cell dies when ionization events occur in its critical structures.

The production of medical radioisotopes depends on several interrelated factors [104]. These include economic feasibility and the availability of starting materials, the delivery chain, the efficiency of radiochemical purification, the level of impurities, and the quantity of radioactive waste generated. The quality of the final product is equally important. In particular, its specific activity and purity depend on the production route selected.

Radioisotopes for radionuclide diagnosis and therapy are currently produced in nuclear reactors and with proton accelerators, primarily cyclotrons. The range of isotopes that can be produced efficiently in reactors is largely limited to uranium fission products such as ^{99}Mo, ^{131}I, and ^{133}Xe and neutron-activation products such as ^{99}Lu and ^{99}Sm. Many promising diagnostic and therapeutic radionuclides cannot readily be obtained in the required quantities by these methods. Isotopes produced by neutron capture, (n, γ), also have low specific activity because nonradioactive carrier atoms remain in the product. This is a critical disadvantage for targeted therapy and has prompted the search for alternative methods.

We are developing a method for producing isotopes through photonuclear reactions. One advantage is that the method can use medical accelerators installed at oncology centers or compact microtrons. Short-lived isotopes can therefore be produced close to the point of care and used immediately for diagnosis and therapy.

Lutetium-177 (^{177}Lu) has attracted substantial scientific and clinical interest as a major theranostic radionuclide because of its distinctive physicochemical properties and successful clinical use [105].

To investigate the feasibility of producing ^{177}Lu with electron accelerators, a series of experiments measured bremsstrahlung-flux-averaged cross sections for photonuclear reactions at endpoint energies of 20, 40, and 55 MeV: ^{181}Ta$(\gamma, \alpha)^{177}$Lu, ^{nat}Hf(γ, pxn), ^{178}Hf$(\gamma, \text{p})^{177}$Lu, ^{179}Hf$(\gamma, \text{pn})^{177}$Lu and ^{180}Hf$(\gamma, \text{p2n})^{177}$Lu [106–112].

Among these reactions, ^{178}Hf$(\gamma, \text{p})^{177}$Lu, particularly with enriched hafnium targets, was found to be the most promising photonuclear route for producing medical ^{177}Lu. Experimental data and calculations performed with TALYS 1.96 [113] were used to estimate the radioactive impurities and stable lutetium isotopes accompanying the target product. Irradiation of enriched ^{178}Hf targets was found to produce no more than 0.3% ^{175}Lu and no more than 1% ^{176}Lu together with ^{175}Lu.

Activity yields were measured experimentally by irradiating targets enriched in ^{178}Hf with bremsstrahlung. At an endpoint energy of 40 MeV, the yield was 2.2×10^5 Bq/(g μA h); at 55 MeV, it was 2×10^5 Bq/(g μA h). These values indicate that irradiating a 100-g ^{178}Hf-enriched target for one hour with a 0.1-mA electron beam can produce approximately 2 GBq of ^{177}Lu. This is comparable with the activities of ^{177}Lu sources used in clinical practice, such as ^{177}Lu-PSMA-617, for which a typical administered activity is approximately 3.6 GBq [114].

The estimated cost of producing ^{177}Lu by the proposed photonuclear method is approximately two orders of magnitude lower than that of the conventional reactor route, ^{176}Lu$(n, \gamma)^{177}$Lu. Several factors account for this difference. First, the natural abundance of ^{178}Hf is 27.28%, substantially greater than the 2.6% abundance of ^{176}Lu in natural lutetium required for reactor production. The latter isotope must also undergo costly enrichment to 82%. Second, no more than 2% of the hafnium target is lost during radiochemical separation of ^{177}Lu, allowing the target to be reused.

These factors demonstrate that electron accelerators and the ^{178}Hf$(\gamma, \text{p})^{177}$Lu reaction on enriched hafnium targets offer a genuinely competitive method for producing medical ^{177}Lu. The resulting isotope combines acceptable specific activity, relatively low cost, high isotopic purity, and substantial logistical advantages.

Studies are also under way to produce the promising radionuclide ^{89}Zr from molybdenum targets with electron accelerators for high-resolution immuno-PET using labeled monoclonal antibodies. Bremsstrahlung-flux-averaged cross sections were measured for photonuclear reactions on zirconium, niobium, and molybdenum targets at endpoint energies of 20, 40, and 55 MeV [115–119]. The most promising photonuclear production route was ^{92}Mo$(\gamma, \text{p2n})^{89}$Nb $\rightarrow$ ^{89}Zr, which provides ^{89}Zr with the highest radionuclidic purity and the lowest content of stable zirconium isotopes.

The activity yields of ^{89}Zr were also measured experimentally by irradiating targets with bremsstrahlung endpoint energies of 20 and 55 MeV. Experimental data and calculations with TALYS 1.96 [113] were used to estimate radioactive impurities and stable zirconium isotopes accompanying the target product. Irradiating 10 g of natural molybdenum for 0.5 h with a 55-MeV endpoint-energy bremsstrahlung beam at a current of 0.4 mA produces enough ^{89g}Nb and ^{89m}Nb that 37 MBq of their daughter isotope ^{89}Zr is present 30 min after the end of irradiation. This activity is sufficient for PET examinations. The fraction of ^{89}Zr nuclei in the $^{89+90}$Zr mixture exceeds 90%. The impurity level, at most $\leqslant 10\%$, has no substantial effect on the sensitivity of radionuclide imaging.

Unlike methods that require enriched targets, the proposed approach can use targets made of natural molybdenum, simplifying production and reducing its cost.

Although photonuclear technologies cannot yet compete with conventional methods in production volume, they offer several fundamental advantages for nuclear medicine. Isotopes can be produced in a decentralized manner on compact electron accelerators located directly in hospitals, and radionuclides can be obtained with high radionuclidic purity and without stable or radioactive isotope contaminants. Photonuclear methods could also help address shortages of critical radioisotopes and facilitate the development of new radiopharmaceuticals for therapeutic use.

Most photonuclear isotope-production centers remain at an early stage of development, but their future potential is increasingly recognized. Several such centers are currently operating worldwide. Leading institutions that study photonuclear reactions and produce isotopes in collaboration with medical centers include TRIUMF in Canada, the Extreme Light Infrastructure — Nuclear Physics facility (ELI — NP) in Romania, Duke University in the United States, and the Kansai Photon Science Institute in Japan. As accelerator technology advances, photonuclear methods may become an important complement to existing methods for producing medical isotopes.

2.7 Development of domestic radiotherapy systems

One practical result of the training provided by our department has been the development of systems for brachytherapy (Fig. 15).

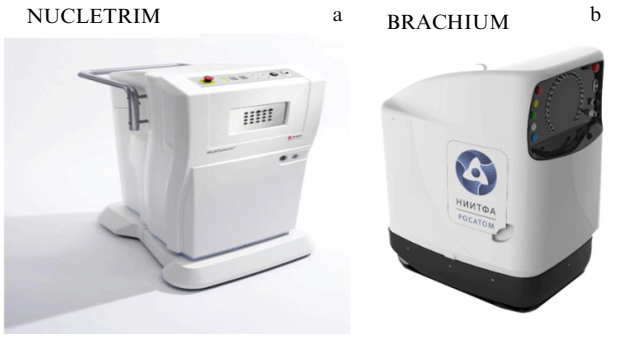

Figure 15. Brachytherapy systems: (a) Nukletrim, developed by MSM; (b) Brachium, developed by NIITFA, Rosatom.

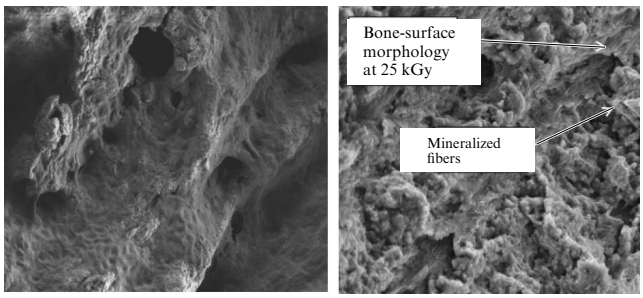

Figure 16. Scanning electron microscopy images of native bone tissue at 5000 magnification before irradiation, left, and after irradiation at 25 kGy, right.

In 2013, working with MSM, we developed Nukletrim, a Russian counterpart to leading German brachytherapy systems. A group of physicists and engineers headed by A.S. Osipov, a member of our department, designed the unit shown in Fig. 15a, improved it relative to its Western counterparts, and raised the proportion of Russian-made components to 50%. Five Nukletrim units are in operation in Russia. Unfortunately, the company subsequently went bankrupt, and the patent was sold to Canada, where the systems are now manufactured. At the Research Institute of Technical Physics and Automation (NIITFA), A.S. Osipov's group later developed another brachytherapy system, Brachium (Fig. 15b). A Russian treatment-planning system was created for Brachium, and more than 70% of its components are manufactured in Russia. Ten Brachium units are currently operating in the country. These systems represent a direct contribution by Moscow State University graduates to the development of radiotherapy in Russia.

Another important healthcare project was implemented jointly with the Radiotherapy Equipment Factory, a subsidiary of R-Pharm. At its facility in Dubna, the company adapted production lines to assemble medical radiotherapy accelerators designed by Varian, one of the leading manufacturers worldwide. More than 100 of these accelerators have been installed in Russia. Our department supported the project by training the required specialists.

3. Radiation sterilization of bone implants, medical devices, and food products

Radiation sterilization has been used for more than 60 years to process food and medical products. X-ray sources, radionuclide devices, and photon and electron beams from charged-particle accelerators are used for this purpose [120].

Combined sterilization of bone implants. Implants are important in the treatment of fractures, trauma, and bone diseases. They include both bone grafts and an expanding range of artificial materials. These materials must be sterilized at room temperature, and clinical practice has shown that implants made from synthetic materials may integrate more successfully.

We are developing a two-component sterilization method that combines ozone with ionizing radiation. This approach improves both implant sterilization and subsequent integration. It also reduces the required radiation dose by a factor of approximately 1.5 and makes the implants more resistant to radiation-induced degradation [121].

The study found no substantial morphological changes in bone tissue after irradiation at doses that ensured complete sterility (Fig. 16).

Combined ozone and radiation sterilization reduces the standard dose of 25 kGy to 11–12 kGy while providing the required sterility and preserving the properties of the bone implant.

We proposed a method for selecting sterilization parameters that ensures the safe use of bone implants in reconstructive surgery while minimizing structural and functional changes in bone tissue. The method provides an effective tissue-preserving technology with potential applications in several biomedical fields.

A system for planning food irradiation with accelerated-electron beams. Food irradiation has been developed to suppress pathogens, insect pests, and bacteria that are hazardous to humans.

We created software that calculates the optimal accelerator settings for a specified product and maximizes the uniformity of irradiation. [5]

An algorithm for reconstructing the electron-beam energy spectrum was developed and tested experimentally. It improves the accuracy of irradiation planning and uses experimentally measured depth-dose distributions as its input data. Industrial irradiation facilities already measure these distributions daily as part of routine operation, so the method requires no additional equipment. It remains stable when the input data contain errors of up to 20%, making it suitable for industrial radiation-processing centers.

The algorithm was implemented in software. An experimentally measured depth-dose distribution is supplied to the program (Fig. 17a), and the energy spectrum of the accelerator's electron beam is reconstructed from it (Fig. 17b) [122].

Extensive experimental studies were used to create a planning system analogous to those employed in radiotherapy. [6] Its performance was verified experimentally on UELR-10-15S and ILU-14 accelerators.

[5] The parameters are the scan width W, electron energy E, scan period T, sweep frequency F_{sweep}, beam-scanning frequency F_{scan}, conveyor speed V_{conv}, accelerator current I, and modifier-plate thickness L.

[6] DEMETRA by IRT, software and database registration certificate, authors A.P. Chernyaev, V.V. Khankin, U.A. Bliznyuk, S.A. Zolotov, and F.R. Studenikin, No. 2023669934, registered September 22, 2023. Dose Preview by IRT, software and database registration certificate, authors A.P. Chernyaev, V.V. Khankin, U.A. Bliznyuk, S.A. Zolotov, and F.R. Studenikin, No. 2023669628, registered September 18, 2023.

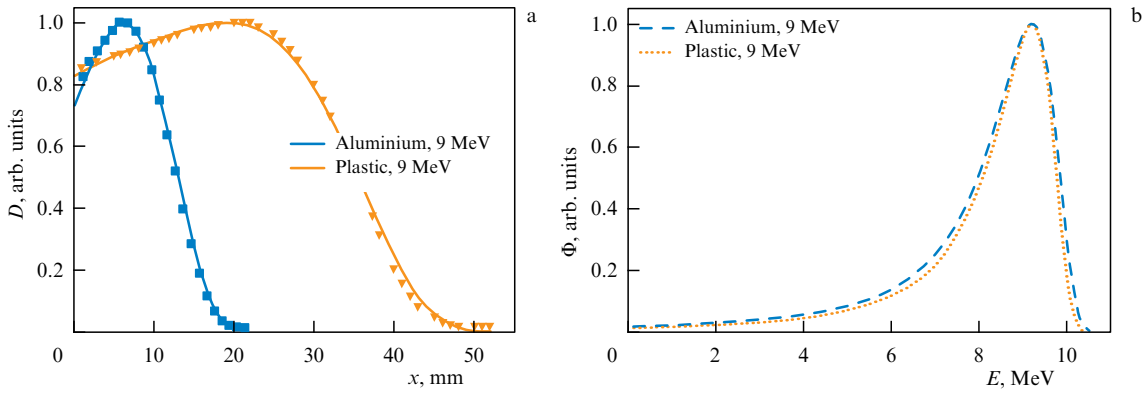

Figure 17. Algorithm for selecting irradiation-mode parameters [122].

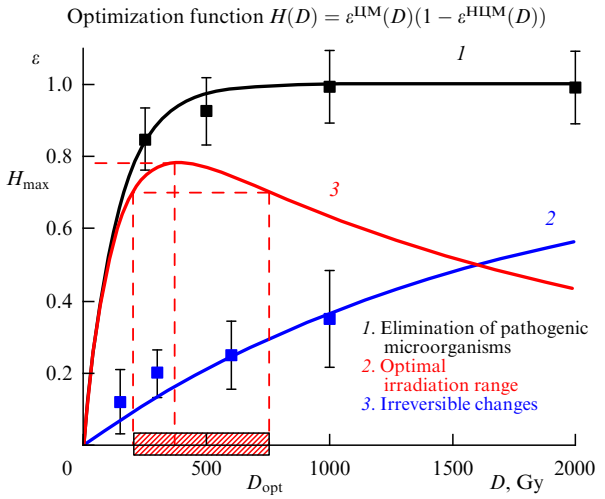

Figure 18. Selection of the optimal dose range for radiation processing of food products [123].

We also proposed a method for selecting the optimal irradiation range that provides microbiological safety while preserving product quality (Fig. 18). Curve *1* in Fig. 18 represents the doses required to destroy all microorganisms; relatively high doses are needed to achieve this result. Curve *2* shows that increasing dose causes irreversible chemical changes in food, reducing its quality and nutritional value. We therefore developed a comprehensive method for selecting a dose range in which the bacteria have been eliminated while product quality remains within the applicable Russian state standards. This effective range is highlighted in red in Fig. 18.

The dose ranges have been determined for different foods and storage periods. Together with the relevant regulatory authorities, we are developing recommendations and standards for food irradiation.

4. A continuous education system for medical physicists

The adoption of advanced technology in Russian healthcare has led medical institutions to employ specialists trained in the natural sciences, including biologists, chemists, physicists, and mathematicians, who perform medical functions together with healthcare professionals. As the amount of high-technology equipment in medical institutions grows, the number of these specialists is rising rapidly. They are needed not only to maintain the equipment but also to operate it.

Approximately 25,000 medical physicists currently work worldwide, compared with 940 in Russia. To reach the level of the leading countries, Russia must increase both its number of medical physicists and its stock of equipment by more than a factor of three. In addition to biology and medicine, these specialists require strong knowledge of nuclear physics, the interaction of ionizing radiation with matter, charged-particle accelerators, dosimetry, and related subjects. Only a few dozen Russian universities train students in nuclear-physics specialties, and the shortage of qualified personnel is particularly acute in the regions.

To provide the country with specialists capable of working with advanced medical systems, Moscow State University established a continuous pathway for educating medical physicists from secondary school through advanced research degrees.

Work with school students. The Faculty of Physics at Moscow State University has organized an outreach system for school students in Moscow. Some senior students undertake research through the University's School for Young Researchers. They can learn about medical physics while still at school and make an informed choice about their subsequent education; some also take their first steps in research. Several participants have later become medical physicists.

Higher education programs and graduate accreditation. For more than two decades, Moscow State University has offered full-time integrated specialist and master's programs in Radiation Medical Physics. More than 220 students have graduated from the department. During their fifth and sixth years, they completed clinical placements in the radiotherapy departments of leading Moscow oncology centers. Graduates receive a higher-education diploma in Physics and a professional-retraining diploma in Medical Physics.

More than 120 graduates of the department's integrated specialist and master's programs now work in oncology centers across Russia.

To be authorized to work with patients as medical physicists under Russian law, graduates must undergo primary specialist accreditation, as physicians do. Moscow State University established the first accreditation center of this kind in 2024.

Continuing education programs. We have also created a range of professional retraining and advanced training programs, aimed primarily at meeting the needs of Russia's regions. Between 2012 and 2025, these programs trained more

Table 2. Continuous education system for medical physicists developed by the Department of Accelerator Physics and Radiation Medicine at the Faculty of Physics of Moscow State University.

Level of education	Program	Number reached or trained
Basic and secondary general education, grades 5–9 and 10–11	Popular-science lectures and podcasts for school students, Radiation Medical Physics	Approximately 2 million
Basic and secondary general education, grades 10–11	School for Young Researchers: School Students' Projects initiative	8
Higher education: integrated specialist degree, bachelor's and master's levels	Integrated specialist program Accelerator Physics and Radiation Medicine; master's program Accelerator Physics and Radiation Medicine; master's program Radiation Medical Physics	220
Continuing professional education	Professional retraining program Medical Physics, 530 h	60
Primary specialist accreditation required to work as a medical physicist Accreditation Commission of Moscow State University		65
Continuing professional education	Advanced training programs: Physics of Radiation Medicine, 90 h; Medical Physics, 144 h; Medical Physics: Treatment Planning, 72 h; Master Class Program for Training Medical Physicists, 30 h; and Methods of Nuclear Medicine, 72 h	159
Periodic accreditation required every five years to continue working as a medical physicist Accreditation Commission of Moscow State University		3
Higher education: training of highly qualified personnel, Candidate of Sciences in Physics and Mathematics	MSU dissertation councils in specialties 1.5.1 Radiobiology; 1.3.15 Physics of Atomic Nuclei and Elementary Particles; High-Energy Physics; and 1.3.18 Physics of Charged-Particle Beams and Accelerator Technology	19
Higher education: training of highly qualified personnel, Doctor of Sciences in Physics and Mathematics	MSU dissertation councils in specialties 1.5.1 Radiobiology; 1.3.15 Physics of Atomic Nuclei and Elementary Particles; High-Energy Physics; and 1.3.18 Physics of Charged-Particle Beams and Accelerator Technology	4
Total number trained in educational programs		498

than 200 specialists from 20 Russian regions[7] and Uzbekistan. Graduates are eligible for primary and periodic accreditation.

Training of highly qualified personnel. Many graduates maintain ties with the University and combine clinical work as medical physicists with research. Over the past 22 years, approximately 30 candidates and doctors of science have defended dissertations on nuclear-physics and radiobiological research for medicine before specialized academic councils at Moscow State University. More than half are medical physicists employed at oncology centers in Moscow and other regions of Russia.

Table 2 summarizes the results of 25 years of work by Moscow State University to train physicists for radiology departments in medical institutions.

Together with the University's graduates, approximately half of all practicing medical physicists in Russia have passed through one or more programs in this educational system. Over more than 25 years, standard textbooks and a dedicated medical-physics library have been produced (Fig. 19). They are used in at least ten Russian universities and five institutions that offer continuing education.

With support from Moscow State University, medical-physics training centers have been established and are developing in Moscow, Moscow Region, Yakutsk, Kazan, Tomsk, Voronezh, and Petrozavodsk, as well as in Tashkent and Samarkand, Uzbekistan (Fig. 20).

[7] Moscow, Moscow Region, Novosibirsk, Donetsk, Orsk, Tomsk, Ryazan, Kirov, Yakutsk, Kaluga, Dimitrovgrad, Chuvashia, Arkhangelsk, Cheboksary, Kemerovo, Abakan, Khanty-Mansiysk, Voronezh, Blagoveshchensk, and Khabarovsk.

Figure 20 shows that specialists trained through this system now work across more than one-third of Russia's vast territory.

The graduates' knowledge and skills are highly regarded by the professional community. Their research has been published in leading high-impact international journals, and the methods developed through this work are already used in oncology institutions in Russia, the United States, the European Union, and other countries.

Despite the scale of the work already completed, the efforts of Moscow State University alone cannot overcome the shortage. Leading universities across Russia must cooperate if the country is to eliminate the staffing deficit and attain a leading position in the number of qualified medical physicists.

The Russian continuous education system presented here compares favorably with its international counterparts and meets current scientific and technological needs. With government support and adoption of this experience across Russia's regions, the shortage of medical physicists could be eliminated within 5–10 years.

5. Conclusion

This review describes the development of Radiation Medical Physics as an educational and research field at Moscow State University and presents a broad range of studies on nuclear-physics technologies for medicine. Joint research with staff from oncology centers has identified several physical factors that increase unaccounted-for doses during cancer treatment. If all of these factors coincide under unfavorable conditions, their combined contribution may reach 9 Gy and increase the risk of secondary cancers by as much as a factor of five.

Textbooks for university programs



The medical physicst library



Figure 19. Textbooks and reference works used to train medical physicists.



Figure 20. Regions of Russia and the Commonwealth of Independent States for which medical physicists have been trained at Lomonosov Moscow State University.

Methods and technologies developed by Moscow State University in collaboration with leading scientific and medical institutions are now used in clinical practice:

— at the Dmitry Rogachev Center, methods for irradiating large tumors and monitoring the dose distribution during a course of radiotherapy;

— at the Burdenko Neurosurgical Institute, a diffusion-weighted imaging method for distinguishing tumor from normal tissue;

— with the Protvino Branch of the Lebedev Physical Institute, a proton-radiography system and a respiratory-motion management system for the Russian proton synchrotron;

— with MSM and NIITFA, the Russian Brachium and Nukletrim medical systems, which are now in clinical operation; and

— photonuclear production of medical isotopes directly at oncology centers using medical electron accelerators or compact microtrons, for which the $^{178}\mathrm{Hf}(\gamma,\mathrm{p})^{177}\mathrm{Lu}$ and $^{92}\mathrm{Mo}(\gamma,\mathrm{p2n})^{89}\mathrm{Nb} \rightarrow {}^{89}\mathrm{Zr}$ reactions have been shown to be competitive routes to $^{177}\mathrm{Lu}$, and $^{89}\mathrm{Zr}$.

Moscow State University has established the only continuous education system in Russia and the Commonwealth of Independent States that extends through doctoral training and dissertation defense. It now reaches 23 regions. New educational and research centers are being created across the country; seven centers for radiation medical physics are already operating in Russia and other CIS countries, and the network continues to expand.

All of this work is directed toward extending the lives of patients with cancer and improving public health.

References

1. Röntgen W C *Science* **3** 227 (1896)
2. Becquerel H *C. R. Hebdomadaires Seances Acad. Sci.* **122** 420 (1896)
3. Grubbe E H *Medical Record* **62** 692 (1902)
4. Curie P, Sklodowska-Curie M *C. R. Acad. Sci.* **127** 1215 (1898)
5. van't Riet A et al. *Int. J. Radiat. Oncol. Biol. Phys.* **37** 731 (1997)
6. Zimmermann R *Nuclear Medicine: Radioactivity for Diagnosis and Therapy* (Les Ulis: EDP Sciences, 2007)
7. Foray N *Int. J. Radiat. Oncol. Biol. Phys.* **96** 717 (2016)
8. Brierley J, Sherman E *Seminars Radiat. Oncol.* **22** 254 (2012)
9. Lister G D, Gibson T *Br. J. Plast. Surg.* **26** 328 (1973)
10. Goodman P C *Am. J. Roentgenol.* **165** 1046 (1995)
11. Huh H D, Kim S *Prog. Med. Phys.* **31** 124 (2020)
12. Colvett K *South Med. J.* **99** 1155 (2006)
13. Christakis P *Yale J. Biol. Med.* **84** 169 (2011)
14. Mohamed M M, Sloane B F *Nature Rev. Cancer* **6** 764 (2006)
15. Krasavin E A *Phys. Usp.* **59** 411 (2016); *Usp. Fiz. Nauk* **186** 435 (2016)
16. Crowther J A *Proc. R. Soc. London B* **100** 390 (1926)
17. Sievert R M *Eine Methode zur Messung von Röntgen-, Radium und Ultrastrahlung: nebst einige Untersuchungen über die Anwendbarkeit derselben in der Physik und der Medizin, mit einem Anhang enthaltend einige Formeln und Tabellen für die Berechnung der intensitätsverteilung bei Gamma-Strahlungsquellen* (Stockholm: Kungl. Boktryckeriet, P.A. Norstedt and Söner, 1932)
18. Lea D E *Actions of Radiations on Living Cells* (Cambridge: The Univ. Press, 1946)
19. Coutard H *Am. J. Roentgenol.* **28** 313 (1932)
20. Klenov G I, Khoroshkov V S *Phys. Usp.* **59** 807 (2016); *Usp. Fiz. Nauk* **186** 891 (2016)
21. Grubbé E *Radiology* **21** 156 (1933)
22. Baltas D, Sakelliou L, Zamboglou N *The Physics of Modern Brachytherapy for Oncology* (Boca Raton, FL: Taylor and Francis, 2007)
23. Maistrenko D N, Granov D A *Voprosy Onkologii* **64** 459 (2018)
24. Sievert R M *Acta Radiologica* **1** 89 (1921)
25. Khlopin V *Usp. Fiz. Nauk* **3** 99 (1922)
26. Radiation Quantities and Units Intern. Commission on Radiological Units and Measurements (ICRU), Report 10a, Handbook 84 (Washington, DC: United States Department of Commerce National Bureau of Standards Library, 1962)
27. Gray L H *Proc. R. Soc. London A* **156** 578 (1936)
28. Sievert R M *Acta Radiol.* **2** 189 (1940)
29. Webster J H D *Proc. R. Soc. Med.* **27** 901 (1934)
30. Coutard H *The Lancet* **224** 1 (1934)
31. Ginzton E L, Nunan C S *Int. J. Radiat. Oncol. Biol. Phys.* **11** 205 (1985)
32. McCready V R *Eur. J. Nucl. Med. Mol. Imaging* **44** 179 (2017)
33. Copeland D E, Benjamin E W *Nucleonics* **5** 44 (1949)
34. Levin V M, Rumyantsev V V *Sov. Atom. Energy* **25** 1271 (1968); *Atom. Energiya* **25** 449 (1968)
35. Johns H E et al. *Nature* **168** 1035 (1951)
36. Slater J M, Miller D W, Archambeau J O *Int. J. Radiat. Oncol. Biol. Phys.* **14** 761 (1988)
37. Larsson B et al. *Nature* **182** 1222 (1958)
38. Alenitsky Y G et al., in *Proc. of the 20th Russian Conf. on Charged Particle Accelerators, RuPAC 2006, Novosibirsk, Russia, September 10–14, 2006* (Eds M Kuzin, E Shirkova) (Novosibirsk: BINP, 2006)
39. Ivanov A A et al. *Phys. Usp.* **65** 834 (2022); *Usp. Fiz. Nauk* **192** 893 (2022)
40. Fowler J F *British J. Radiol.* **38** 365 (1965)
41. Hounsfield G N *British J. Radiol.* **46** 1016 (1973)
42. Ambrose J *British J. Radiol.* **46** 1023 (1973)
43. Leksell L *Acta Chir. Scand.* **134** 585 (1968)
44. Lauterbur P C *Nature* **242** 190 (1973)
45. Mansfield P *J. Phys. C* **10** L55 (1977)
46. McCullough E C, Krueger A M *Int. J. Radiat. Oncol. Biol. Phys.* **6** 1599 (1980)
47. Cunningham J R *Int. J. Radiat. Oncol. Biol. Phys.* **16** 1367 (1989)
48. Favaudon V et al. *Sci. Transl. Med.* **6** 245 (2014)
49. Bulanov S V et al. *Phys. Usp.* **57** 1149 (2014); *Usp. Fiz. Nauk* **184** 1265 (2014)
50. Kravchuk L V *Phys. Usp.* **53** 635 (2010); *Usp. Fiz. Nauk* **180** 665 (2010)
51. Matveev V A *Phys. Usp.* **67** 1180 (2024); *Usp. Fiz. Nauk* **194** 1250 (2024)
52. Akulinichev S V *Phys. Usp.* **57** 1239 (2014); *Usp. Fiz. Nauk* **184** 1363 (2014)
53. Ng J, Shuryak I *Cancer Manag. Res.* **7** 1 (2014)
54. Thwaites D, Baldock C *J. Phys. Conf. Ser.* **444** 011001 (2013)
55. Hall E J, Wuu C-S *Int. J. Radiat. Oncol. Biol. Phys.* **56** 83 (2003)
56. Chernyaev A et al. *Quantum Beam. Sci.* **7** 27 (2023)
57. Kamran S C et al. *Cancer* **122** 1809 (2016)
58. de Gonzalez A B et al. *Lancet Oncol.* **12** 353 (2011)
59. Kim T J et al. *Cancers* **13** 1144 (2021)
60. Atli E et al. *Diagnostic Intervent. Rad.* **27** 1147 (2021)
61. Sodickson A et al. *Radiology* **251** 175 (2009)
62. Dalah Z et al. *Clin. Pract.* **14** 1550 (2024)
63. Cao C-F et al. *BMC Cancer* **22** 1238 (2022)
64. Nievelstein R A J et al. *Eur. Radiol.* **22** 1946 (2012)
65. Verfaillie G et al. *EJNMMI Phys.* **10** 32 (2023)
66. Brix G et al. *Eur. J. Nucl. Med. Mol. Imaging* **41** S125 (2014)
67. Grewal R K et al. *J. Nucl. Med.* **51** 1361 (2010)
68. Huang B, Law M W M, Khong P L *Radiology* **251** 166 (2009)
69. Alshamrani A F A, Alrehily F A *JRRAS* **18** 101303 (2025)
70. Murat H et al. *Radioprotection* **60** 65 (2025)
71. Fabritius G et al. *Sci. Rep.* **6** 35181 (2016)
72. Schöder H, Gönen M *Nucl. Med.* **4** 18 (2007)
73. Ben-Sellem D, Ben-Rejeb N *Nucl. Med. Mol. Imaging* **55** 173 (2021)
74. Hosono M et al. *British J. Radiol.* **94** 1126 (2021)
75. Chawla S C et al. *Pediatr. Radiol.* **40** 681 (2010)
76. Lykova E N et al. *Moscow Univ. Phys. Bull.* **79** 524 (2024); *Vestn. Mosk. Univ. Ser. 3 Fiz. Astron.* (4) 2440703 (2024)
77. Torfeh T et al. *Magn. Reson. Imaging* **34** 645 (2016)
78. Jezzard P *Neuroimage* **62** 648 (2012)
79. Lu L et al. *J. Appl. Clin. Med. Phys.* **24** e13843 (2023)
80. Wang D, Doddrell D M *Curr. Med. Imaging. Rev.* **1** 49 (2005)
81. Gantsovskii P P et al. *Izv. Ross. Akad. Nauk. Ser. Fiz.* **84** 1547 (2020)
82. Chernyaev A P, Lykova E N, Shcherbakov A A *Nanobiotechnol. Rep.* **18** 617 (2023)
83. Lykova E N "Issledovanie potokov vtorichnykh chastits pri rabote meditsinskogo uskoritelya s energiei 18–20 MeV" ("Investigation of secondary particle fluxes during the operation of a medical accelerator with an energy of 1820 MeV"), PhD Thesis (Phys. and Math. Sci.) (Moscow: Lomonosov Moscow State Univ., 2019)
84. Hall E J *Int. J. Radiat. Oncol. Biol. Phys.* **65** 1 (2006)
85. Romero-Expósito M, Toma-Dasu I, Dasu A *Front. Oncol.* **12** 892078 (2022)
86. Takam R et al. *Radiat. Res.* **176** 508 (2011)
87. Kinoshita N et al. *Radiol. Phys. Technol.* **18** 58 (2025)
88. Yock A D et al. *Pract. Radiat. Oncol.* **9** 200 (2019)
89. Takahashi Y et al. *Sci. Rep.* **15** 3608 (2025)
90. Du W et al. *J. Appl. Clin. Med. Phys.* **17** 167 (2016)
91. Hansen E K et al. *Int. J. Radiat. Oncol. Biol. Phys.* **64** 355 (2016)

92. Bortfeld T et al. *Phys. Med. Biol.* **47** 302 (2002)
93. Lykova E N et al. *Izv. Ross. Akad. Nauk. Ser. Fiz.* **86** 557 (2022)
94. National Research Council. 2006. Health Risks from Exposure to Low Levels of Ionizing Radiation: BEIR VII (Washington, DC: The National Academies Press, 2006)
95. Li C I et al. *Cancer Res.* **70** 7187 (2010)
96. Preston D L *Cancer Spectrum Knowledge Environment* **94** 1555 (2002)
97. Neglia J P et al. *J. Natl. Cancer Inst.* **98** 1528 (2006)
98. Zubkov M A et al. *Phys. Usp.* **62** 1214 (2019); *Usp. Fiz. Nauk* **189** 1293 (2019)
99. Jena R et al. *Clin. Oncol.* **17** 581 (2005)
100. Loginova A A et al. *Front. Oncol.* **12** (2022)
101. Belikhin M et al. *Phys. Med.* **112** 102612 (2023)
102. Zavestovskaya I N, Kolobov A V, Ryabov V A *Phys. Usp.* **67** 866 (2024); *Usp. Fiz. Nauk* **194** 917 (2024)
103. Belikhin M A "Razrabotka i issledovanie metoda kompensatsii dvizheniya opukholei v protonnoi terapii skaniruyushchim puchkom" ("Development and research of the method for compensating the movement of tumors in proton therapy with a scanning beam"), PhD Thesis (Phys. and Math. Sci.) (Moscow: Lomonosov Moscow State Univ., 2023)
104. Zhuikov B L *Phys. Usp.* **59** 481 (2016); *Usp. Fiz. Nauk* **186** 544 (2016)
105. Dyachkov A B et al. *Phys. Usp.* **66** 518 (2023); *Usp. Fiz. Nauk* **193** 554 (2023)
106. Zheltonozhskaya M V et al. *Nanobiotechnol. Rep.* **18** 577 (2023)
107. Zheltonozhsky V A et al. *Nucl. Instrum. Meth. Phys. Res. B* **476** 68 (2020)
108. Zheltonozhsky V A et al. *Bull. Russ. Acad. Sci. Phys.* **84** 923 (2020); *Izv. Ross. Akad. Nauk. Ser. Fiz.* **84** 1116 (2020)
109. Zheltonozhsky V A et al. *Eur. Phys. J. A* **57** 121 (2021)
110. Zheltonozhskiy V A et al. *Bull. Russ. Acad. Sci. Phys.* **86** 1083 (2022); *Izv. Ross. Akad. Nauk. Ser. Fiz.* **86** 1305 (2022)
111. Zheltonozhskaya M V et al. *Phys. Part. Nucl. Lett.* **20** 1433 (2023); *Pis'ma Fiz. Elem. Chast. Atom. Yad.* **20** 1471 (2023)
112. Zheltonozhskaya M V et al. *Phys. Atom. Nucl.* **86** 917 (2023); *Yad. Fiz.* **86** 641 (2023)
113. Koning A J, Rochman D *Nucl. Data Sheets* **113** 2841 (2012)
114. Kabasakal L et al. *Mol. Imaging Radionucl. Therapy* **26** 62 (2017)
115. Zheltonozhskaya M V et al. *Radiat. Phys. Chem.* **224** 112082 (2024)
116. Remizov P D et al. *Phys. Atom. Nucl.* **85** 818 (2022); *Yad. Fiz.* **86** 99 (2023)
117. Zheltonozhskaya M V, Remizov P D, Chernyaev A P *Appl. Radiat. Isotop.* **199** 110871 (2023)
118. Remizov P D et al. *Eur. Phys. J. A* **59** 141 (2023)
119. Remizov P D et al. *Bull. Russ. Acad. Sci. Phys.* **87** 1112 (2023); *Izv. Ross. Akad. Nauk. Ser. Fiz.* **87** 1092 (2023)
120. Bryazgin A A, Kuksanov N K, Salimov R A *Phys. Usp.* **61** 601 (2018); *Usp. Fiz. Nauk* **188** 672 (2018)
121. Nikolaeva N et al. *Int. J. Mol. Sci.* **24** 14426 (2023)
122. Zolotov S A et al. *Phys. Scr.* **100** 045020 (2025)
123. Shik A V et al. *Food Chem.* **482** 144073 (2025)